

Internal Electric Field Structure of Launched Fast Magnetosonic Waves in the DIII-D Tokamak

J. H. Lee,^{1,2} W. A. Peebles,¹ E. F. Jaeger,³ E. J. Doyle,¹ N. C. Luhmann, Jr.,⁴ C. C. Petty,⁵ R. I. Pinsker,⁵
R. Prater,⁵ and T. L. Rhodes¹

¹*Department of Electrical Engineering and Institute of Plasma and Fusion Research, University of California, Los Angeles, California 90095*

²*School of Electronic and Electrical Engineering, Hong-Ik University, Seoul 121-791, Korea*

³*Oak Ridge National Laboratory, Oak Ridge, Tennessee 37831*

⁴*Department of Applied Science, University of California, Davis, California 95616*

⁵*General Atomics, P.O. Box 85608, San Diego, California 92186*

(Received 21 March 1996)

Results are obtained, for the first time in a major tokamak plasma, of the spatial electric field structure of a launched fast magnetosonic wave (FW). The FW launch directionality necessary for current drive has been confirmed at a position close to the FW antenna. The FW electric field profile is determined using X-mode reflectometry. Electric field profiles, calculated using a full-wave numerical code, exhibit many features common to the experimental results. However, differences remain regarding density dependence that suggest alternative damping mechanisms may exist. [S0031-9007(98)05541-0]

PACS numbers: 52.50.Gj, 52.55.Fa

Fast magnetosonic wave current drive (FWCD) is an attractive method to obtain steady-state or long pulse operation in a tokamak fusion reactor [1–3]. FWCD is achieved when the fast magnetosonic wave (FW) transfers momentum to electrons by the coherent combination of electron Landau damping and transit time magnetic pumping, i.e., FW damping to electrons [4,5]. Fast waves in the ion cyclotron range of frequencies can easily penetrate to the center of plasmas with high density and temperature. On DIII-D, FWCD is being utilized to achieve and maintain advanced tokamak performance [6] necessary to construct a compact, efficient steady-state tokamak reactor. Encouraging results from DIII-D have supported the feasibility of this advanced operational regime [7].

Extensive theoretical analysis has been performed for FWCD; models and theory predict wave number, wave trajectory, electric field profile, FW absorption/damping, FW deposition profile, current drive efficiency, etc. [8,9]. However, little experimental data exist regarding FW propagation inside a hot fusion plasma. Determination of the FW electric field profile is extremely important as it can be directly related to code and model results providing validation and benchmarking. Such knowledge can also enhance our understanding leading to improvements in both the control and efficiency of rf heating and current drive. It should be noted that a highly directional FW launched spectrum is essential in order to efficiently drive current. Prior to the results presented herein, no direct confirmation of the directionality of the launched FW inside a plasma has been available. Evidence of directionality had previously been restricted to external rf loop measurements [10] and measurement of the current drive itself [11].

In this Letter, the internal spatial structure of the FW electric field is determined, for the first time in a major tokamak plasma, using an internal, nonperturbing, and

spatially localized reflectometry technique [12]. The FW antenna launch directivity in the DIII-D tokamak has been experimentally determined at a position close to the antenna. The reflectometer signal is enhanced when the fast wave is launched directed towards the detection position using $(0, \pi/2, \pi, 3\pi/2)$ phasing of the four strap antenna. Determination of the FW electric field profile using a full-wave code (PICES) [9] is found to have many common features with the experimental results: The launch directivity is observed and the electric field decreases towards the edge. However, differences remain regarding the density dependence of the calculated and experimentally determined profiles which suggest that some additional FW damping, independent of density, is required to explain this discrepancy. The measured FW damping time in plasmas with small single pass damping has also been studied and is observed to be shorter than linear theoretical estimates of FW electron Landau damping would indicate [5]. This also suggests that more damping is occurring than expected in these discharges. Possible reasons for the differences between experiment, theory, and code are discussed in more detail later.

An internal and nonperturbing diagnostic (X-mode reflectometry) has been employed to locally monitor the coherent fluctuations in density and magnetic field induced by the FW electric field inside the plasma. The reflection position (right-hand cutoff) for X-mode propagation [13] depends on electron density (n_e) and magnetic field (B) and responds to local changes in n_e and B . The FW modulates the local density and magnetic field at the launched FW frequency (60 MHz). A frequency tunable (~ 65 – 73 GHz) heterodyne X-mode reflectometer is located at the mid-plane, 9.5 cm toroidally away from the edge of the last current strap of the FW antenna. The reflectometer has frequency tunability for spatial scanning, and, most importantly, total reflected power monitoring at the intermediate

frequency (IF) for signal normalization purposes. The system employs heterodyne tracking receiver techniques [14] to eliminate electromagnetic pickup and to stabilize the IF frequency. In the DIII-D system, the coherent modulations driven by the FW fields are then detected as sidebands of the IF using the above system.

Using the electron continuity equation in the cold plasma approximation and slab geometry ($k_\theta = 0$), the amplitude of the density and magnetic fluctuations induced by the FW field can be approximated as

$$\frac{\tilde{n}_e}{n_e} \cong \frac{k_r}{\omega} \frac{\tilde{E}_\theta}{B_t} \cong \frac{\tilde{B}_z}{B_t} \propto \frac{n_e^{0.5}}{B_t^2} \tilde{E}_\theta. \quad (1)$$

Here, \tilde{E}_θ is the FW electric field, \tilde{B}_z is the dominant FW magnetic field, and \tilde{n}_e is the resulting density fluctuation. These terms are time varying at the FW frequency ω . The subscripts r , θ , and z represent the radial, poloidal, and toroidal directions, respectively. The FW radial wave number is k_r , n_e is the plasma electron density, and B_t is the toroidal magnetic field. It is noted that ω/k_r can be approximated as the Alfvén velocity ($\propto B_t/n_e^{0.5}$). For long wavelength perturbations (e.g., the FW perpendicular wavelength of ~ 10 cm is much larger than the reflectometer probe wavelength of ~ 0.5 cm), a geometric optic approach is appropriate for interpreting reflectometer signals [15,16]. In this limit, the reflectometer signal is clearly localized to the cutoff layer [15]. It should be noted that the FW reflectometer signal depends not only upon the local FW power, but also upon the power in the microwave beam, the mixer conversion loss, and propagation and refraction. In order to remove these, the total reflected power, which also depends upon these effects, is monitored at the intermediate frequency of $f_{IF} = 200$ MHz and used to normalize the FW sideband signal at a frequency $f_{IF} + f_{FW} = 260$ MHz, since the measurement utilizes heterodyne detection. Adopting this approach and using Eq. (1), the *normalized* reflectometer signal (S) can be related to \tilde{n}_e/n_e and \tilde{E}_θ as indicated below:

$$S \propto \left[\frac{f_0(1 + f_{ce}f_0/f_p^2)}{1/L_n + (f_{ce}f_0/f_p^2)/L_B} \right]^2 \frac{n_e}{B_t^4} \tilde{E}_\theta^2, \quad (2)$$

where L_n and L_B are, respectively, the density and magnetic field gradient scale lengths, f_{ce} is the electron cyclotron frequency, f_p is the electron plasma frequency, and f_0 is the reflectometer probe frequency. The detailed density profile was obtained via high repetition rate multipoint Thomson scattering. Note that all of the above parameters, except for \tilde{E}_θ , are experimentally determined.

FWCD experiments on DIII-D utilize a four-strap phased antenna array [17] to establish the toroidal propagation direction of the coupled FW spectrum. The FWCD efficiency is unambiguously related to the directivity of the launched spectrum. In this section, direct experimental evidence is presented that a directed FW is, in fact, launched from the above antenna. The determined FW local power ($\propto \tilde{E}_\theta^2$) is enhanced for a fast wave launched

towards the detection position using $(0, \pi/2, \pi, 3\pi/2)$ antenna phasing, as compared to $(0, -\pi/2, -\pi, -3\pi/2)$ phasing, as shown in Fig. 1(b). The monitored total reflected powers at the IF are shown in Fig. 1(c) and are similar in both cases, indicating that the difference is indeed related to the antenna directivity. The measured signal ratio for the two antenna phasings from Fig. 1(b) is ~ 6.7 during the period of constant density (1600–2000 ms). A detailed interpretation of this ratio is somewhat complicated as the measured signal is generated by several possible launched FW components, which can mutually interfere. They consist of the main lobe FW component launched from the antenna to the reflectometer detection position, a side lobe (reverse direction) component, as well as contributions from *multiple* toroidal passes, which exist due to the relatively weak expected absorption. Thus, the ratio $P_{-\pi/2}/P_{\pi/2}$ can be represented as

$$\frac{P_{-\pi/2}}{P_{\pi/2}} = \frac{A_b^2 + A_{i-\pi/2}^2}{A_f^2 + A_{i\pi/2}^2} = 0.15 \text{ (measured)}, \quad (3)$$

where $P_{\pm\pi/2}$ are the FW reflectometer signal powers with $(0, \pm\pi/2, \pm\pi, \pm 3\pi/2)$ phasings. A_f is the coupled wave amplitude for the forward (main lobe) direction, A_b is the coupled wave amplitude for the reverse (side lobe) direction, and $A_{i\pm\pi/2}$ is the FW component that results from one or more toroidal transits in the $(0, \pm\pi/2, \pm\pi, \pm 3\pi/2)$ phasing. Here, it is assumed

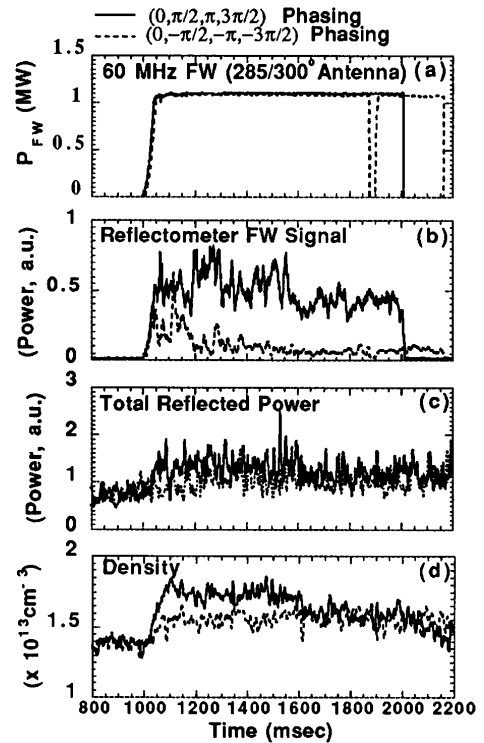


FIG. 1. (a) Net coupled fast wave power. (b) Time evolution of unnormalized fast wave reflectometer signal power. (c) Time evolution of *total* reflected reflectometer signal power ($I_p = 1.4$ MA, $B_t = 2.1$ T, $T_{e0} \sim 5$ keV, deuterium discharge). (d) Line averaged density.

that the interference terms average to zero during the averaging interval (1600–2000 ms) because a small change (~2%) in density generates one interference pattern. Taking the worst case scenario, $A_{i\pi/2} = A_f$ and $A_{i-\pi/2} = 0$, produces a lower bound of 54% on the coupled directivity where directivity is defined as $(A_f^2 - A_b^2)/(A_f^2 + A_b^2)$.

The FW electric field profile was determined during a density ramp where $\langle n_e \rangle$ varied from $\sim 2.2 \times 10^{19} \text{ m}^{-3}$ to $\sim 3.2 \times 10^{19} \text{ m}^{-3}$ within a single shot. As the density rises, the position of the right-hand cutoff layer moves radially outwards towards the plasma edge, e.g., the 73 GHz reflectometer detection position moves from 2.14 to 2.27 m. Figure 2 shows the FW electric field profiles determined using this method. The plasma was a double null divertor configuration with plasma current $I_p = 0.8 \text{ MA}$ and toroidal magnetic field $B_t = 2.1 \text{ T}$. The reflectometer probe frequency was scanned from shot-to-shot using reproducible plasmas. As can be seen, the determined FW electric field ($\propto \tilde{E}_\theta^2$) profiles were all similar and all decreased toward the plasma edge for different probe frequencies. The FW launch toroidal directivity is also clearly observed. As can be seen, the FW electric field profiles are relatively insensitive to electron density, since the various profiles illustrated in Fig. 2 were determined using different reflectometer probe frequencies. For example, the data taken at $R = 2.2 \text{ m}$ at 67 and 73 GHz differ locally in density by ~40%. It should also be stressed that a separate profile obtained in a constant density plasma using a shot-to-shot frequency scan displayed similar spatial characteristics.

Figure 3(a) illustrates the FW electric field (\tilde{E}_θ^2) profile calculated using the PICES full-wave code [9] for similar discharge plasma parameters as in Fig. 2. The calculated single pass absorption is 10.5% for these plasmas. The FW electric field profile is obtained by averaging five electric field profiles obtained over a range of density [$n_{e0} = (2.2\text{--}2.6) \times 10^{19} \text{ m}^{-3}$]. As can be seen, the calculated profiles exhibit many common features with the

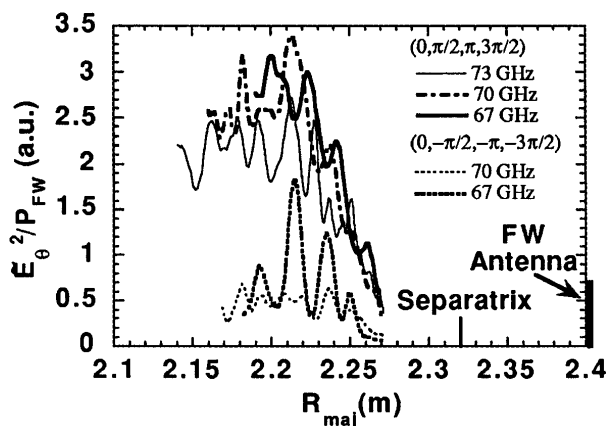


FIG. 2. Experimentally determined FW electric field profiles ($\propto E_\theta^2$) are illustrated for $(0, \pm\pi/2, \pm\pi, \pm 3\pi/2)$ antenna phasings using different reflectometer probing frequencies ($I_p = 0.8 \text{ MA}$, $B_t = 2.1 \text{ T}$, $T_{e0} \sim 5 \text{ keV}$, deuterium discharge).

experimental results, i.e., the launch directionality is observed and the electric field decreases towards the edge.

Figure 3(b) shows the FW electric field profile calculated by averaging profiles obtained over a range of density of $(2.7\text{--}3.1) \times 10^{19} \text{ m}^{-3}$. At these higher densities, the resulting single pass absorption increases by 4%, since the electron Landau damping is proportional to electron density ($\propto n_e^{1.5}$). As can be seen in Fig. 3, the code results are very sensitive to electron density. On the other hand, the experimental data were seen to be relatively insensitive to electron density, as shown in Fig. 2. This discrepancy suggests that some additional damping, insensitive to electron density, exists in the experiment. Another observation is that a small scale structure, consistent with fast wave interference effects, is found in both experiment and in code calculations. However, the spatial scales are different in experiment and theory. The scale in theory is ~9 cm, which corresponds to the half wavelength of FW, while the scale in the experiment is ~2 cm. This scale difference is thought to be due to movement of the detection position as the density increases. This causes an increase in the number of minima and maxima counted. It should be noted that the structure in the experiment is not due to interference effects of microwave radiation used by the reflectometer since this would result in much smaller (~0.3 cm) spatial variations.

The decay time of the reflectometer signal was also measured as the FW power was terminated in order to obtain a measure of the FW damping time. The turn-off times of

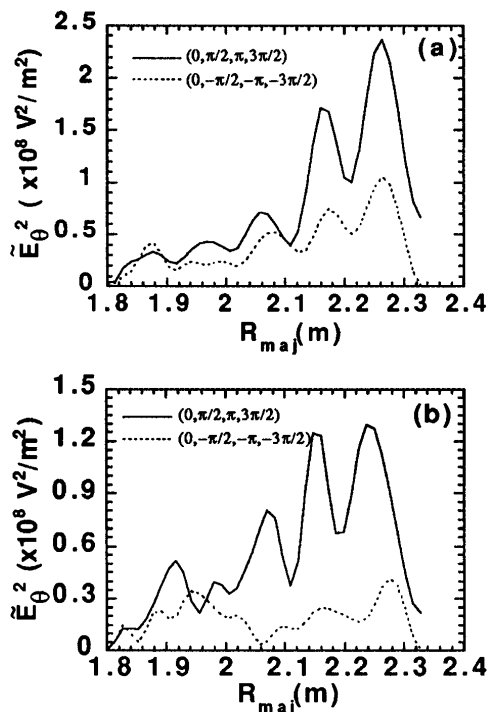


FIG. 3. (a) The calculated FW electric field profile (E_θ^2) from the PICES full-wave code using parameters similar to the experiment over a range of density $n_{e0} = (2.2\text{--}2.6) \times 10^{19} \text{ cm}^{-3}$; (b) over a range of density $n_{e0} = (2.7\text{--}3.1) \times 10^{19} \text{ cm}^{-3}$.

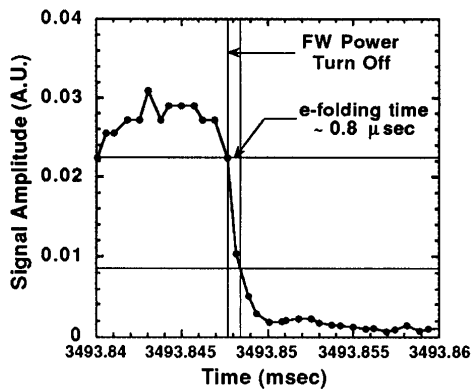


FIG. 4. Measured reflectometer FW signal decay time. ($I_p = 1$ MA, $B_t = 1.9$ T, $\langle n_e \rangle \sim 2.1 \times 10^{19} \text{ m}^{-3}$, $T_{e0} \sim 1.4$ keV, and $k_{\parallel} = 9.6 \text{ m}^{-1}$ at plasma center, deuterium discharge).

the launched rf power and the reflectometer system were ~ 0.6 and $\sim 0.4 \mu\text{sec}$, respectively. In these high temperature ($T_{e0} \sim 5$ keV) plasmas, since the calculated [5] FW damping time was within the measurement uncertainty, it was decided to also study a lower temperature plasma ($T_{e0} \sim 1\text{--}2$ keV), where a much longer damping time is predicted. However, even in this lower temperature case, an e -folding time of $\sim 0.8 \mu\text{sec}$ was measured as illustrated in Fig. 4. The detection position was $\rho \sim 0.5$. Linear theory predicts a damping time due to electron Landau damping using these experimental parameters ($B_t = 1.9$ T, $\langle n_e \rangle \sim 2.1 \times 10^{19} \text{ m}^{-3}$, $T_{e0} \sim 1.4$ keV, and $k_{\parallel} = 9.6 \text{ m}^{-1}$ at plasma center) of $\sim 20 \mu\text{sec}$. The details regarding this discrepancy are not fully understood. However, a possible explanation is that additional damping mechanisms and/or enhanced FW damping to electrons (e.g., more upshift and/or broadening of the k_{\parallel} spectrum than expected) are occurring.

As suggested above, the differences between experiment and theory/code can be explained by invoking other possible damping mechanisms. First, one possible additional FW damping mechanism is that due to the finite cavity Q of the vessel. This effect has not been included in the current full-wave code and theoretical analysis. If this is the dominant damping mechanism, then it is important that FWCD be performed in a high single pass absorption regime so that the losses to the wall become negligible. The overall FWCD efficiency would, of course, then increase significantly. The second possibility is that there is more upshift and/or broadening of k_{\parallel} [18] than expected. This would cause the resonance condition ($\omega - k_{\parallel} v_{\parallel e} = 0$) to move to lower electron temperatures, and the associated FW electron Landau damping to increase. Third, some experimentally unknown parameter, e.g., a higher hydrogen concentration near the second harmonic cyclotron layer (located near plasma center at 2.1 T), could introduce additional damping. Fourth, FW power may be coupled to the slow wave branch via the parametric decay process or mode conversion to ion Bernstein waves. Parametric decay has previously been observed on DIII-D, but it was estimated to be a small ($< 1\%$) loss per pass [19].

In summary, the FW electric field profile has been determined in the DIII-D tokamak through the measurement of coherent fluctuations induced by FW electric fields. The directional capability of the FW launch antenna has been directly verified experimentally at a position close to the FW antenna. Comparison of the determined FW electric field profile with a full-wave code during $(0, \pm\pi/2, \pm\pi, \pm 3\pi/2)$ antenna phasing indicated many common features. The spatial profile of the FW electric field is observed to decay towards the plasma edge which is consistent with the full-wave calculations. However, differences remain regarding the density dependence of profiles that suggest alternative damping mechanisms may also be at work. The measured FW damping time in low single pass absorption plasmas is observed to be much shorter than linear theory predicts, also indicating the need for additional damping mechanisms.

The authors gratefully acknowledge the work and support of the DIII-D team. This work is supported by U.S. DOE Grant No. DE-FG03-86ER53225 and Contracts No. DE-AC03-89ER51114 and No. DE-AC05-84OR21400.

- [1] R. Prater *et al.*, *Plasma Phys. Controlled Fusion* **35**, A53 (1993).
- [2] R.I. Pinsker *et al.*, *Plasma Physics and Controlled Fusion Research (Proceedings of the 14th International Conference, Wurzburg, Germany, 1992)* (IAEA, Vienna, 1993), Vol. I, p. 683.
- [3] Equipe Tore Supra, in *Proceedings of the 15th International Conference on Plasma Physics and Controlled Fusion Research, Seville, Spain, 1994* (IAEA, Vienna, 1995).
- [4] T. H. Stix, *Nucl. Fusion* **15**, 737 (1975).
- [5] M. Porkolab, in *Radiofrequency Power in Plasmas, Proceedings of the Ninth Topical Conference, Charleston, SC, 1991* (American Institute of Physics, New York, 1992), p. 197.
- [6] A. D. Turnbull *et al.*, *Phys. Rev. Lett.* **74**, 718 (1995).
- [7] L. L. Lao *et al.*, *Phys. Rev. Lett.* **70**, 3435 (1993); J. R. Ferron *et al.*, *Phys. Fluids B* **5**, 2532 (1993); P. A. Politzer *et al.*, *Phys. Plasmas* **1**, 1545 (1994).
- [8] S. C. Chiu *et al.*, *Nucl. Fusion* **29**, 2175 (1989).
- [9] E. F. Jaeger *et al.*, *Nucl. Fusion* **33**, 179 (1993).
- [10] R. Prater *et al.*, *Fusion Eng. Des.* **26**, 49 (1995).
- [11] C. C. Petty *et al.*, *Nucl. Fusion* **35**, 773 (1995).
- [12] J. H. Lee *et al.*, *Rev. Sci. Instrum.* **66**, 1225 (1995).
- [13] V. L. Ginzburg, *The Propagation of Electromagnetic Waves in Plasmas* (Pergamon, New York, 1970).
- [14] J. L. Doane, *Rev. Sci. Instrum.* **51**, 317 (1980).
- [15] N. Bretz, *Phys. Fluids B* **4**, 2414 (1992).
- [16] A. Mase *et al.*, *Phys. Fluids B* **5**, 1677 (1993).
- [17] R. H. Goulding *et al.*, in *Radiofrequency Power in Plasmas, Proceedings of the Ninth Topical Conference, Charleston, SC, 1991* (American Institute of Physics, New York, 1992), p. 287.
- [18] H. Ikezi *et al.*, "Fast Wave Propagation Studies in the DIII-D Tokamak," *Phys. Plasmas* (to be published).
- [19] J. R. Myra and D. A. D'Ippolito, *Bull. Am. Phys. Soc.* **39**, 1628 (1994).